Golden Goal Collaborates with Flamingo in Conferring Synaptic-Layer Specificity in the Visual System

Satoko Hakeda-Suzuki, Sandra Berger-Mueller, Tatiana Tomasi, Tadao Usui, Shin-Ya Horiuchi, Tadashi Uemura, Takashi Suzuki

Golden Goal Collaborates with Flamingo in Conferring Synaptic-Layer Specificity in the Visual System

Satoko Hakeda-Suzuki[1,4], Sandra Berger-Müller[1,4], Tatiana Tomasi[1], Tadao Usui[2], Shin-ya Horiuchi[2], Tadashi Uemura[2,3] and Takashi Suzuki[1,5]

[1]Max Planck Institute of Neurobiology

Am Klopferspitz 18

D-82152 Martinsried

Germany

[2]Graduate School of Biostudies

Kyoto University

Kyoto 606-8507

Japan

[3]Japan Science and Technology Agency

CREST

Kyoto 606-8507

Japan

[4]These authors contributed equally to this work

[5]Corresponding author: Tel:+49-89-8578-3449, E-mail:suzukit@neuro.mpg.de

Running Title: Gogo and Fmi specify synaptic-layer targeting

SUMMARY

Neuronal connections are often organized in layers, which contain synapses between neurons that have similar functions. In *Drosophila*, R7 and R8 photoreceptors, which detect different wavelengths, form synapses in distinct medulla layers. The mechanisms underlying the specificity of synaptic-layer selection remain unclear. We found that Golden Goal (Gogo) and Flamingo (Fmi), two cell-surface proteins involved in photoreceptor targeting, functionally interact in R8s. Our genetic studies indicated that Gogo promotes R8 adhesion to the temporary layer M1, whereas Gogo and Fmi collaborate to mediate axon targeting to the final layer M3. Structure-function analysis suggests that Gogo and Fmi interact with intracellular components through the Gogo cytoplasmic domain. Moreover, Fmi is also required in a subset of target cells for R8 axon targeting. We propose that Gogo acts as a functional partner of Fmi for R8 axon targeting and that the dynamic regulation of their interaction specifies synaptic-layer selection of photoreceptors.

INTRODUCTION

The establishment of well-defined synaptic connections between specific neurons is critical for information processing in the brain. Synapses are often arranged into structures which reflect a functional organization of synaptic contacts[1-2]. In the visual system for instance, nearby photoreceptors connect to nearby columns in the target region, preserving the spatial relationships between the visual world and its representation in the brain[1, 3]. In addition to this retinotopic organization, different features of a visual stimulus are often decoded into separate synaptic layers[2-3]. These characteristic columnar and layered structures are often seen in complex nervous systems. How do axons select their specific synaptic layer during

development? The mechanisms underlying the formation of synaptic layers are still unclear, although important molecular players have been identified[2-4]. In the vertebrate visual system, several homophilic adhesion molecules, such as Sidekicks and Dscams, play a crucial role in layer-specific targeting of photoreceptors by utilizing their binding specificity[3, 5-6].

Synaptic connections in the *Drosophila* visual system are also organized in layers, and synaptic specificity is well investigated in this system. The Drosophila compound eye is made of about 800 units called ommatidia, each containing eight photoreceptors (R1-R8). R1-R6 axons mediate motion detection and project to the first optic ganglion, the lamina. The photoreceptors responsible for color vision, R7 and R8, innervate the second optic ganglion, the medulla[7-8]. Each pair of R7 and R8 axons that mediates information from the same point in space forms a columnar structure in the medulla. Importantly, R7 and R8, which respond to different wavelengths, connect to separate medulla layers (M6 and M3, respectively). Thus distinct functional modularities become processed in distinct synaptic layers. Therefore, the *Drosophila* visual system provides an attractive model to study synaptic-layer selection[3, 7-9].

In *Drosophila*, several transmembrane molecules have been shown to regulate synaptic-layer targeting of photoreceptors. Examples include N-Cadherin[10-11], two receptor tyrosine phosphatases, LAR[11-13] and PTP69D[11, 14-15], a cell adhesion molecule Capricious (Caps)[16-17] and a putative receptor Golden goal (Gogo) [11, 18]. Although the requirement of each of these proteins has been reported, it is not fully understood how synaptic-layer specificity is achieved by this set of proteins.

Additionally, the seven-pass transmembrane cadherin Flamingo (Fmi) has an important function in axon pathfinding of photoreceptors and is potentially implicated in layer-specific targeting[11, 19-20]. Fmi also regulates dendrite formation and planar cell polarity (PCP)[21-22]. In R axon guidance, the primary role of *fmi* is regulating afferent-afferent interaction in larva and lamina cartridge formation[19-20, 23]. Fmi mediates homophilic binding *in vitro*[21], however the molecular mechanism of *fmi* in axon pathfinding remains unclear.

In this study, we first show that Fmi has a specific role in synaptic-layer targeting independent of afferent-afferent interaction. We further asked how the targeting specificity of R8 axons is achieved by Fmi. The broad expression of Fmi in all R axons and in multiple target layers suggests that Fmi does not achieve R8 targeting specificity alone. The phenotypic similarities between *gogo* and *fmi* suggested that Gogo might be a functional associate of Fmi that adds the specificity code required for R8 synaptic-layer targeting. Although we could not demonstrate a direct physical interaction, our results show that Gogo and Fmi can mutually affect their localizations and that they functionally interact in R8s. Our genetic data indicated that Fmi may interact antagonistically with Gogo at the M1 temporary layer, and that Gogo and Fmi cooperate to mediate targeting of R8 axons to M3. We also show that the intracellular signaling for synaptic-layer specificity is primarily mediated by the cytoplasmic domain of Gogo. Finally, the requirement of Fmi in the brain for R8 axon targeting suggested that Fmi in R axons homophilically interacts with Fmi in the target cells.

Taken together, these results indicate that Gogo and Fmi are functional partners in axon guidance, and that their collaboration specifies the synaptic-layer choice of R8 axons. We propose that synaptic-layer specificity is achieved by combinatorial codes of cell-surface molecules.

RESULTS

Fmi regulates synaptic-layer targeting

To demonstrate that Fmi has a role in synaptic-layer targeting of R8 axons independent of the axon-axon bundling defect seen in larvae [19-20], we generated single *fmi* mutant R8 axons to minimize axon bundling. Single $fmi^{-/-}$ R8 axons showed targeting defects and abnormally stopped at the M1 layer in the adult medulla **(Fig. 1a–d,k)**.

To assess the requirement of *fmi* in pupae when R8 layer-targeting occurs, we removed *fmi* during pupal stages. To achieve this, we used the temperature sensitive repressor Gal80[ts] system[24] to control the *fmi* transgene expression. The initial *fmi* expression driven at 27°C was sufficient to rescue the R axon bundling phenotype of the *fmi* mutant in the larval stage **(Supplementary Fig. 1)**. Late third instar larvae were then transfered to 18°C to shut down *fmi* expression. In the adult, we observed severe R8 targeting defects, albeit the bundling phenotype and the overall structure of the medulla was rescued **(Fig. 1e–g)**. Together, we showed that *fmi* has a role in synaptic-layer targeting which is independent of its earlier function in axon-axon interaction.

Fmi cytoplasmic domain is dispensable for R8 axon targeting

To determine whether Fmi can transmit the guidance signal inside the growth cone, we tested if the cytoplasmic domain of Fmi is required for R8 axon pathfinding. To do so, we developed a strategy to make a conditional knock-out of *fmi*. We used FLPase and available FRT lines flanking *fmi* to flip-out *fmi*. This technique is referred to as FRTs located in *cis* for conditional knock-out (FLICK) throughout this study **(Supplementary Fig. 2**, see **Methods)**. Using this method, we knocked out *fmi* specifically in the eye with eyFLP, and we could rescue the *fmi* mutant phenotype with Fmi lacking its intracellular domain (FmiΔIntra transgene) **(Fig. 1h–j)**. Since the cytoplasmic domain of Fmi is dispensable, Fmi may have other interactors to convey the guidance signal intracellularly.

We tested whether core PCP complex proteins[25], which are known to interact with Fmi, have any role in R8 axon targeting. Mutant R8 axons for *frizzled* (*fz*), *van gogh* (*vang*, also known as *strabismus*), *dishevelled* (*dsh*) and *prickle* (*pk*) showed completely normal targeting, suggesting that PCP proteins do not play a role in R8 axon targeting (**Supplementary Fig. 3a–d**).

gogo and *fmi* have similar neuronal phenotypes

Previous studies reported that *gogo* mutants show R8 pathfinding and targeting defects[18] that are similar to those in *fmi* mutants. To check whether these phenotypes in adults result from the same defects during development, we compared *gogo* and *fmi* mutants at different pupal stages. R8 axons target their synaptic layer in a two-step manner [26]: they first halt at the temporary layer M1 until 50APF, and then start extending filopodia to their final target layer M3. Like in *gogo* mutants, the majority of R8 axons fail to send filopodia towards the M3 target layer at this stage in *fmi* mutants[18] (**Supplementary Fig. 4**). Additionally, *gogo* mutants have similar defects to *fmi* mutants[19, 23] in R1-6 synaptic target selection in lamina cartridges (**Fig. 2a,b,e**). These defects in *gogo* mutants are not secondary to the R8 axon pathfinding phenotype, since R1-6 target selection is still abnormal when R8s are specifically rescued in *gogo* mutants (**Fig. 2c–e**). Moreover, we found that *gogo* mutants show similar defects to *fmi* mutants in dendrite formation of embryonic md neurons[22, 27]. Dendrites overgrew and 8.3% of the segments showed dorsal midline crossing (**Fig. 2f–h**). However, the functions of these two proteins do not perfectly overlap, since the *gogo* mutant does not exhibit a PCP phenotype[18] (**Supplementary Fig. 3e–g**). The similarities between *gogo* and *fmi* neuronal phenotypes suggested that *gogo* and *fmi* may act in the same pathway during neuronal development.

In addition, Gogo and Fmi showed striking similarities in their expression patterns (**Fig. 2i–u**). Especially in R axons in the third instar larval optic lobe, Gogo and Fmi stainings essentially overlapped (**Fig. 2i–q**). Similarly to Fmi[19], Gogo strongly localized to the youngest axons which innervate the outmost part of the crescent shape of the optic lobe (**Supplementary Fig. 5**). Notably, Fmi was also strongly expressed in the target region, whereas Gogo was mainly detectable in R axons in third instar larvae and throughout the first half of pupal stages **(Fig. 2r–u)**. Altogether, despite some small differences, the striking similarities in the neuronal phenotype and the overlapping expression patterns suggested that Fmi interacts with Gogo in the development of the nervous system.

gogo and *fmi* interact genetically in neuronal development

As a first indication of *gogo* and *fmi* genetic interaction, we observed the impact of the mutations on the lethality. The *fmi* hypomorphic mutation (*fmi*[E86]/*fmi*[E59]) reduced the survival rate to 16.2%. Removing one copy of *gogo* in this background resulted in a further reduction of the survival rate to around 5% **(Fig. 3a)**, suggesting a cooperation of these two genes.

To further assess the genetic interaction between *gogo* and *fmi*, we overexpressed both proteins under the control of the photoreceptor specific driver GMR-Gal4. We used a moderate *gogo* overexpression line, UAS-*gogo*T1[18]. When Gogo or Fmi were overexpressed separately, R7 axons targeted the proper layer M6 (**Fig. 3b-d**). When both proteins were co-overexpressed, however, almost half of R7 axons stopped at the M3 layer where R8 axons normally terminate (**Fig. 3b,e**). This effect was not observed when Fz, an interactor of Fmi[28], was co-overexpressed with Fmi, suggesting that the synergistic effect between Gogo and Fmi is specific (**Supplementary Fig. 6**). To test whether this redirecting phenotype still occurs with R7 specific expression, we overexpressed Gogo and Fmi in R7s, but not in R8s, using

the GMR-FLP technique (see Methods). Although the penetrance was reduced (possibly due to the perdurance of the Gal80 repressor protein), we still observed R7 mistargeting to M3 (**Fig. 3b,f**). This suggests that Gogo and Fmi act together to recognize and to adhere to the M3 target layer.

We further tested the genetic interaction in the loss-of-function situation. To exclude the contribution of Fmi from the brain, we used the FLICK system to generate a *fmi* hypomorphic mutant only in R axons, with the rest of the animal remaining wild type (*fmi*[E86]/+) (see Methods). In these flies, R8s only occasionally innervated neighboring medulla columns and made abnormal contacts with other R8 axons (**Fig. 3g,i**). The incidence of the R8 defects increased significantly when one copy of *gogo* was removed in the *fmi*[E86] hypomorphic background (**Fig. 3h,i**). This suggests that *gogo* and *fmi* genetically interact in R8 neurons in the loss-of-function situation.

If *fmi* and *gogo* act in the same genetic pathway, we should not see an additive effect in the double mutant. The double knock-out of *fmi* and *gogo* using the *ey*FLP-FLICK system showed a failure of R8s to target M3 layer; rather, R8s stay at the M1 layer like in the *fmi* mutant (**Fig. 3j-l**, see **Methods**). There is a slight difference in the way R8s interact with the M1 temporary layer (**Supplementary Fig. 7**, see also discussion), however the phenotype of R8s failing in extending their filopodia to the M3 layer at 55APF (After Puparium Formation) are very similar among *gogo*, *fmi* single and the double mutants (**Supplementary Fig. 4**). Altogether, these results suggest that *gogo* and *fmi* function in the same pathway when R8 targets the M3 layer, and their collaboration confers specificity to the synaptic-layer selection of R8 axons.

We also observed a robust genetic interaction in dendrite formation. The dorsal-midline crossing phenotype in the *fmi* hypomorph mutant (15.3% per segment) was significantly enhanced by removing one copy of *gogo* (29.6%) (**Fig. 3m–p**). This indicates

that *gogo* and *fmi* collaborate not only in axons but also more generally in neuronal processes including dendrites.

Gogo and Fmi colocalize at cell-cell contacts in S2 cells

S2 cells transfected with Fmi form aggregates due to Fmi homophilic interactions, and Fmi often accumulates at sites of cell-cell contacts. The transmembrane PCP proteins Vang and Fz have been shown to colocalize with Fmi at boundaries between adjacent cells [29]. When Gogo and Fmi were co-transfected, Gogo was enriched at sites of cell contacts together with Fmi (**Fig. 4a–c,p**). This effect was specific to Gogo and Fmi, since neither Gogo accumulated with another cadherin E-Cad (**Fig. 4d–f,p**), nor did Unc5[30], another transmembrane receptor which structurally resembles Gogo, co-accumulate with Fmi (**Fig. 4g–i,p**). We found that Gogo colocalizes with Fmi without the cytoplasmic portion of both proteins, indicating that colocalization is mediated by their transmembrane or extracellular domains (**Fig. 4j–l,p**). A chimeric protein consisting of the extracellular domain of Gogo and the transmembrane and cytoplasmic domains of Unc5 ($Gogo^{Ecto}$::$Unc5^{TM+Cyto}$) colocalized with Fmi at cell-cell contacts (**Fig. 4m–o,p**), suggesting that the ectodomain of Gogo mediates the colocalization with Fmi.

To investigate whether Gogo and Fmi mediate heterotypic interaction in *trans*, we performed an aggregation assay by mixing Gogo-expressing cells with Fmi-expressing cells. Cells transfected with Gogo were not more included in the aggregates generated by Fmi than the control cells transfected with mCD8 (**Supplementary Fig. 8a,b**), which suggests that Gogo and Fmi interact in *cis*.

Gogo and Fmi interact in *cis in vivo*

To assess the interaction of Gogo and Fmi *in vivo*, we used the wing epithelial cells, which have well-organized cell borders where Fmi accumulation is easily visible. At mid-pupal stage (28APF), Fmi is normally localized apically at adherens junctions on the proximal and distal borders. When we ectopically overexpressed Gogo, Fmi localization was disrupted at the apical pole of the cells (**Fig. 5a,c**) and Fmi was relocated to the entire surface of lateral membranes (**Fig. 5b,d**) without disrupting adherens junction components (**Supplementary Fig. 9**). This suggested that Gogo binds and recruits Fmi to the baso-lateral membrane (**Fig. 5e**).

We then tested if Gogo could relocalize Fmi in *trans* or in *cis*, by generating *fmi* mutant clones. Fmi was not relocalized to the basolateral membrane of the abutting cells when *fmi* was absent from the *gogo*-overexpressing cells (**Fig. 5f–i**), suggesting that Gogo does not interact with Fmi in *trans* (**Fig. 5j**). On the contrary, Fmi in Gogo-overexpressing cells was still relocalized on lateral cell membranes abutting *fmi* mutant cells (**Fig. 5k–n**), which indicates that Gogo relocates Fmi in *cis* (**Fig. 5o**). These data support our hypothesis of the physical interaction between Gogo and Fmi (direct or indirect) and indicate that they interact in *cis*.

Gogo accumulation at the growth cone is dependent on Fmi

We next tested whether Gogo and Fmi localizations are reciprocally dependent on each other also in growing R axons. We found that, in *fmi* mutant R axon growth cones, Gogo accumulation is reduced compared with the surrounding wild type axons (**Fig. 5p–s**). This strongly indicates that Gogo and Fmi interact endogenously in R axon growth cones, and that it stabilizes Gogo accumulation. It is noteworthy that Gogo localization at the growth cone is not completely dependent on Fmi, since at 24APF, we could detect Gogo accumulation at $fmi^{-/-}$ R growth cones (**Supplementary Fig. 10a–d**).

We did not, however, observe a mutual dependency of Gogo or Fmi localization at the cell body and along the axonal shaft of photoreceptors, and Fmi accumulation in *gogo* mutant R axon tips was normal (**Supplementary Fig. 10e–m**). Thus, it seems that the trafficking and the transport of Gogo and Fmi to the axons occur mostly independently of each other, and that they only interact at the tip of axons after transport.

Gogo cytoplasmic domain is crucial for the M3 targeting

Since FmiΔIntra could rescue the R8 axon targeting defects, it is possible that the interacting partners of Fmi convey the signal received by Fmi ectodomain to the intracellular space. As Gogo interacts with Fmi in axon pathfinding, and since GogoΔC cannot rescue the *gogo* mutant phenotype in R axon targeting [18], we anticipated that Gogo may transduce guidance information inside the growth cone.

To test this, we used the experiment of *gogo* and *fmi* overexpression in R neurons, which showed R7 redirecting to the M3 layer (see **Fig. 3e**). When we overexpressed both FmiΔIntra and GogoΔC, R7 extended normally to the M6 layer, suggesting that Gogo and Fmi interact with intracellular components (0.0% at 25°C; **Fig. 6a,d** and **Supplementary Fig. 11a,b,g**). Overexpression of Fmi full length and GogoΔC resulted only in a subtle R7 premature stopping phenotype (7.2% at 25°C; **Fig. 6b,d**), whereas FmiΔIntra and Gogo full length overexpression induced a much stronger phenotype (41.0% in 25°C; **Fig. 6c,d**). The expression level of each of these transgenes was comparable (**Supplementary Fig. 11c–f**). Therefore, we concluded that Gogo and Fmi transmit the M3 targeting information to downstream components primarily through the cytoplasmic domain of Gogo. This indicates that intracellular transduction of the axon guidance signal may be the major role of Gogo when it collaborates with Fmi.

Fmi is required in the target area for R8 axon targeting

Fmi functions through homophilic interaction both *in vivo* and *in vitro*. We wondered whether Gogo and Fmi in R8 axons bind to Fmi on the target cells to achieve the proper innervation of R8s. It was shown using the ELF system that Fmi seems to be required in the target area, but the outcome was somewhat modest (5.6% bundling, 0.4% stopping) [31].

Using a variety of Gal4 lines driving FLPase in lamina and/or medulla neurons, we used the FLICK system to knock out *fmi* in the target area. Among them, *gcm*-Gal4 FLICK flies showed robust R8 axon targeting defects (**Fig. 7a,c** and **Supplementary Table 1**). As monitored by *Act*<stop<*nLacZ* [32], FLP-out occurred in a subset of brain cells including almost all lamina neurons, but not in R cells (**Fig. 7b**). In *gcm*-Gal4 *fmi* FLICK flies, Fmi expression was indeed strongly reduced in the medulla at early and mid-pupal stages (**Fig.7d–w**). The morphology of the medulla neuropiles seems to be normal (**Fig. 7h,m,r,w,x** and **Supplementary Fig. 12**). The requirement of Fmi in the brain strongly suggests that Gogo and Fmi on R8 axons interact with Fmi in target cells in *trans* (**Supplementary Fig. 13a**).

Fmi antagonizes Gogo adhesion to the M1 temporary layer

From the *in vivo* co-overexpression data, the interaction between Gogo and Fmi seems to specifically mediate M3 layer recognition of R8 axons. In our former work, we showed that Gogo overexpression induces a stronger affinity of R8 axons to the M1 layer [18]. How can this be explained? We hypothesized that there might be a different function of Gogo and Fmi when R8 interacts with the temporary M1 layer. We tried to address this issue by changing the balance of Gogo and Fmi activity level in R8 axons. We first overexpressed *gogo* in *fmi*

hypomorph R8s. If the Gogo overexpression phenotype (blob-like structure at M1) is also mediated by Fmi, the M1 blobs would be suppressed by the partial removal of *fmi*. We observed, however, the opposite effect: more R8s stopped at the M1 layer compared to the moderate *gogo* overexpression or the *fmi* hypomorphic mutant phenotypes **(Fig. 8a-d)**.

On the contrary, when the expression of *fmi* was mildly elevated (with GMR-*fmi*) in the Gogo overexpression situation, M1 blobs were strongly reduced **(Fig. 8e–g)**. This suggests that Gogo alone promotes adherence to the M1 layer, but when Gogo interacts with Fmi at the mid-pupal stage, Fmi inhibits the Gogo-M1 interaction, and Gogo and Fmi act together to mediate R8 association with the M3 layer **(Supplementary Fig. 13b)**. Whereas the ligand on the M3 layer is likely to be Fmi, the presumptive ligand on the M1 layer is unknown. Thus, it seems that there exists a complicated regulation of the Gogo-Fmi interaction and that Gogo alone has a different function than when it is associated with Fmi.

DISCUSSION

Interaction between Gogo and Fmi

In this study, we have suggested that the transmembrane receptor Gogo physically interacts (directly or indirectly) with the atypical cadherin Fmi in *cis* to cooperatively guide R8 axons to their correct target. However, we have been unable to demonstrate a robust direct interaction between Gogo and Fmi by coimmunoprecipitation, Bimolecular Fluorescent Complementation (BiFC)[33] or Proximity Ligation Assay (PLA)[34] **(Supplementary Figs. 14 and 15,** see also **Supplementary Note 1)**. The failure in coimmunoprecipitation is probably due to technical difficulties in solubilizing the seven-pass transmembrane Fmi and maintaining a huge complex during the procedure (Fmi is about 400 kD). Nevertheless, a close interaction of these proteins is supported by three lines of evidence. First, ectopic

expression of Gogo in wing epithelial cells is able to relocate Fmi in *cis*. Second, Fmi and Gogo colocalize at cell-cell contacts in cultured cells via their ectodomains. Finally, Gogo accumulation at the growth cone is strongly reduced in *fmi* mutant R axons, suggesting that Fmi is at least partially required to localize/stabilize Gogo at the growth cone through a close association.

It has been suggested that Fmi binds homophilically in *cis* [27]. We also found that Gogo forms oligomers in cultured cells (**Supplementary Fig. 8e**). These observations suggest that even if Gogo and Fmi physically interact with each other, they may multimerize and form a protein cluster. Alternatively, Gogo-Gogo, Gogo-Fmi and Fmi-Fmi interactions may happen separately at distinct locations and have different functions.

Gogo and Fmi in neuronal development

Fmi controls the nervous system development broadly. It regulates axon guidance, but also synaptic target selection and dendritic field development [22-23, 27, 35-37]. The phenotypic similarities and the genetic interactions of *gogo* and *fmi* in diverse aspects of neuronal development in *Drosophila* suggest that the collaboration of Gogo and Fmi is a general molecular mechanism.

Interestingly, however, in the dendrites of multi-dendritic neurons, it has been reported that the ectodomain deletion of Fmi (FmiΔN) is able to partially rescue the *fmi* dorsal-overgrowth phenotype in dendrites, but FmiΔC cannot [27]. On the contrary, in R8 axons, FmiΔN cannot rescue (**Supplementary Fig. 16**), but FmiΔIntra can (**Fig. 1j**). These observations indicate that the underlying molecular mechanisms may be different between axons and dendrites. It will be therefore interesting to investigate the molecular mechanisms of Gogo in dendrite formation to decipher the general principles versus unique, diversified mechanisms mediated by the Gogo-Fmi interaction.

Mechanisms of axon targeting by the Gogo-Fmi interaction

What is the function of Gogo when interacting with Fmi? We can envision three scenarios that are not mutually exclusive. First, Fmi homophilic adhesion properties change when it is associated with Gogo. Second, Gogo mediates intracellular signaling to transduce axon pathfinding information in the growth cone. Third, Gogo adds a specificity code to the Fmi-Fmi homotypic asymmetric interaction. To test the first scenario, we used a cell aggregation assay mixing Fmi-expressing cells with cells co-expressing Gogo and Fmi. Since the two populations of cells were equally distributed in the aggregates **(Supplementary Fig. 8c,d)**, Gogo seems not to have an effect on Fmi homophilic adhesion in S2 cells. The second scenario is supported by the fact that the Gogo cytoplasmic domain mediates the R7 co-overexpression phenotype, and that Fmi cytoplasmic domain is dispensable for R8 axon pathfinding. Additionally, the interaction between Gogo and Fmi seems to add molecular specificity to R8 axons, allowing them to recognize the proper layer M3, suggesting the third scenario. Fmi seems to be the "cue" on the target layers, since elimination of Fmi from a population of brain cells, but not from photoreceptors, resulted in targeting defects in R8 axons. This suggests that Fmi-Fmi homotypic interactions take place between R8 axons and the target cells **(Supplementary Fig. 13a)**. However, the interaction seems to be asymmetric, since Gogo is not required in the brain for R axon pathfinding [18].

Overall, we propose that: 1) Gogo alone promotes adherence between R8 axons and the M1 layer [18]**(Supplementary Fig. 13b)**; 2) at mid-pupal stages, Fmi acts antagonistically with Gogo at the M1 layer, and Gogo and Fmi collaborate to mediate R8 targeting to the M3 layer **(Supplementary Fig. 13b)**; 3) at the M3 layer, Fmi on the target cells mediates homophilic interaction with Fmi on R8 axons **(Supplementary Fig. 13a)**. Fmi could be detected on R8 axons when R8s extend their tip to the M3 layer, if Fmi protein level was

reduced from surrounding neuropils, consistent with the idea that Gogo and Fmi act together to guide the M3 targeting growth cones (**Supplementary Fig. 17**). The above model is supported by mainly five lines of evidence: 1) co-overexpression of Fmi and Gogo retargets R7 axons to the M3 layer (**Fig. 3e,f**), 2) removing Fmi from presumptive target cells induces R8 stopping at the M1 layer (**Fig. 7a**), 3) a combination of Gogo overexpression and *fmi* hypomorphic background induces more R8 axon stopping at M1 layer than each of these genotypes individually (**Fig. 8c**), 4) the Gogo overexpression phenotype is suppressed by mild *fmi* overexpression (**Fig. 8e**). Taking into account that *gogo* overexpression in a *fmi* hypomorph could not enhance the axon bundling which is typical in *fmi* mutant axons, it is unlikely that *gogo* overexpression acts merely as dominant-negative on Fmi function. 5) In *fmi* mutants, R8 commonly stalls at the M1 layer, whereas in *gogo* mutants[18] or in the double mutants, R8 has a tendency to stray at the M1 layer (**Supplementary Fig. 7**). We think that this difference is due to a reduced adhesion of R8 to M1 in *gogo* mutants, which is not impaired in *fmi* mutants.

The cell identity of the M3 layer which is recognized by Gogo and Fmi in R8 axons is not clear. We knocked-out *fmi* almost completely from the lamina neurons. Although the R8 stopping phenotype is not completely penetrant, we see substantial R8 stopping at the M1 layer, indicating that the lamina neurons might be the target cells where Fmi functions as a ligand. Lamina neurons innervate into medulla layers during early pupal stages. Their processes take over R8 axons when R8 axons rest at the temporary layer, and they arborize between developing R7 and R8 termini [26, 38]. Interestingly, L3 lamina neurons spread their terminal processes at the M3 layer [39] (see also **Fig. 7x**). The functional significance of L3 neurons in this context should be addressed in the future. In any case, it seems that mutual interactions between lamina neuron processes and R axons account for the two step targeting mechanism of R8 axons [26, 38].

LEGENDS

Figure 1 *fmi* regulates synaptic-layer targeting and does not require its cytoplasmic domain. (**a**) Horizontal image of the wild type adult medulla. R axons are labeled with mAb24B10 (red), R8 axons with *Rh6*-GFP (green) and medulla-layers with anti-N-Cad (blue). Medulla layers are indicated by white dashed lines. (**b**,**c**) Images of *ey*3.5FLP $fmi^{-/-}$ mosaic adult medulla. WT axons are labeled with GMR-mCD8mKOrange (red), R8 axons with *Rh6*-GFP (green) and medulla layers with anti-N-Cad (blue). Single $fmi^{-/-}$ R8 axons (green without red) abnormally stopped at the M1 layer (arrows). The quantification of the phenotype of single $fmi^{-/-}$ R8 axons is shown in **d**. (**e**–**g**) Temporal $fmi^{-/-}$rescue using Gal80[ts]. The eye specific $fmi^{-/-}$ mutants were generated by FLICK (see **Supplementary Fig.2**) and the *fmi* transgene was expressed using *ey3.5*FLP, *Act*<CD2<Gal4 and UAS-*fmi*. The expression level of the *fmi* transgene was controlled by *tub*-Gal80[ts]. The labeling is identical to **a**. The $fmi^{-/-}$ phenotype was rescued at 27°C (**e**) whereas there was no rescue at 18°C (**g**). (**f**) When the temperature was shifted from 27°C to 18°C at the late third instar larval stage, R8 axons abnormally stopped at M1 (arrows). (**h**–**j**) $fmi^{-/-}$ *ey*3.5*FLP* FLICK (**h**) was successfully rescued by GMR-Gal4 UAS-*fmi* (**i**) or by GMR-Gal4 UAS-*fmi*ΔIntra (**j**). The labeling is identical to **a**. (**k**) Schematics of the optic lobe development. Representative individual neurons are depicted in blue, whereas neuronal regions are color coded (retina: yellow; lamina: green; medulla: red). Scale bars represent 20μm.

Figure 2 Phenotypic similarities between *gogo* and *fmi*. (**a**–**c**) EM sections of lamina cartridges. R axons are colored in green. (**a**) WT, (**b**) *gogo*[D1600] *ey*FLP mosaic mutant, (**c,d**) R8 specific rescue of *gogo*[D1600] *ey*FLP using 109-68-Gal4 and *caps*-Gal4. Note that R7/8 axon pathfinding is largely rescued (**d**). (**e**) Distribution of the number of R1−R6

terminals per cartridge of *gogo* mutants (black bars), *gogo* R8 specific rescue (dark gray bars) and control eyes (light gray bars). (**f**,**g**) Dorsal view of 20-22AEL (After Egg Laying) embryonic md neurons in the WT (**f**) and *gogo*[D869]/[H1675] (**g**). Dendrites are labeled with 109(2)80-Gal4 UAS-GFP. *gogo* mutant dendrites show a midline crossing phenotype (arrowheads in **g**). (**h**) Quantification of the longest dendritic branch from md neurons in the WT (gray bars) and in the *gogo* mutant (black bars). (**i**–**k**) Gogo (green) and Fmi (magenta) expression in late third instar larva. Gogo and Fmi distributions overlap in R axons and their terminals. Note that both Fmi and Gogo localize strongly in the youngest R axons (arrows). (**l**–**n**) Magnification of the region shown in **i**. R axons marked with *glass*-LacZ (red in **o**–**q**), overlap with the Fmi (white in **p**) or Gogo signal (white in **q**). (**r-t**) Gogo (green) and Fmi (magenta) expression in 24 APF pupa. At this stage, Gogo and Fmi are expressed in R axons, but Fmi becomes more apparent in brain neuropils between R7-R8 axons (white brackets). (**u**) Magnification of the region shown in **r**. The scale bars represent 2μm (**a**) and 20μm (**f, i**, **r**).

Figure 3 *gogo* genetically interacts with *fmi*. (**a**) Survival rates of the indicated genotypes. (p=0.00025 Chi-Test). (**b**–**f**) The gain-of-function interaction between *fmi* and *gogo* was tested using GMR-Gal4, UAS-*fmi* and/or UAS-*gogo*. (**b**) Quantification of the R7 axons mistargeting to M3 at 20°C (gray) or 25°C (black). (**c**–**e**) R7 axons are labeled with *Rh4*-GFP (green), together with 24B10 (red) and N-Cad (blue). R7 axons target normally when *fmi* (**c**) and *gogo* (**d**) are overexpressed separately. (**e**) Co-overexpression induces R7 mistargeting to the M3 layer (arrows) (20°C). Note that eye morphology is severely disrupted at 25°C, thus not applicable (N.A. in **b**). (**f**) R7 specific clones overexpressing *gogo* and *fmi* were marked by GFP (green) using GMR-FLP. R7s frequently stop at M3 (arrows). (**g**–**h**) R8 bundling phenotype in the *ey*3.5FLP *fmi*[E86] FLICK mutant with $gogo^{+/+}$ (**g**) or with $gogo^{+/-}$ (**h**).Traces of R8 axons in focus (black), out of focus (gray) and the points of R8 axon

bundling (arrows) are shown below each panel. (**i**) Quantification of R8 axon bundles within a defined thickness ($p<0.0001$ two tailed t-test). (**j–l**) *ey3.5*FLP mediated FLICK mutants of *gogo* (**j**), *fmi* (**k**) and *gogo*, *fmi* double knock-out (**l**). (**m–p**) ClassIV dendrites of 20-22 AEL embryos in the WT (**m**), the *fmi* hypomorph (**n**), and the *fmi* hypomorph with $gogo^{+/-}$ (**o**). (**p**) Quantification of ClassIV dendrites crossing the midline ($p= 0.00064$ Chi-Test). The labeling in **g,h,j-l** is the same as in **Figure 1a.** Scale bars represent 20μm.

Figure 4 Gogo and Fmi colocalize at cell-cell contacts. (**a–o**) Protein accumulation at cell boundaries in transienlty transfected S2 cells subjected to aggregation assay. All cells are co-transfected with the *Act*-Gal4 driver. Cells co-transfected with Fmi and Gogo-myc (**a–c**), E-cad-GFP and Gogo-myc (**d–f**), Fmi and Unc5-GFP (**g–i**), FmiΔC-myc and GogoΔC-GFP (**j–l**), and Fmi and $Gogo^{Ecto}$::$Unc5^{TM+Cyto}$-GFP (**m–o**). Fmi recruits Gogo at cell-cell contacts (**a–c**), whereas Gogo does not colocalize with E-cad (**d–f**), nor does Unc5 colocalize with Fmi (**g–i**). FmiΔC can recruit GogoΔC (**j–l**) and Fmi recruits the chimera $Gogo^{Ecto}$::$Unc5^{TM+Cyto}$ (**m–o**), which suggests that the ectodomains of Gogo and Fmi mediate their colocalization. (**p**) Quantifications of the accumulation of each protein are shown on the right side of each panel. The cell-cell contact accumulation ratio is the ratio of the fluorescence intensity at the cell-cell border to the fluorescence intensity at the membrane which does not contact other cells. The sample size is indicated with n.

Figure 5 Gogo interacts with Fmi in *cis* in wing cells. (**a–d,f–i,k–n**) Images of *gogo*-overexpression clones in 28 APF wing cells from the apical surface (**a,c,f,h,k,m**) and 5 μm beneath the surface (**b,d,g,i,l,n**). (**a–d**) Subcellular localization of Gogo-myc (**a,b**) and Fmi (**c,d**) is detected with anti-Myc and anti-Fmi. The clone border is marked with a white line. At the apical surface, the proximo-distal localization of Fmi becomes disrupted in *gogo*-overexpressing clones (**c**). More basally, Fmi localizes on the lateral membrane of wing cells

(arrows in **d**), similarly to Gogo (**b**). A schematic explanation is shown in **e**. (**f–i**) Overexpression of *gogo* in *fmi* mutant clones. Fmi does not localize on the membrane of Gogo-overexpressing cells between fmi^{+} and fmi^{-} cells (**g,i**), indicating that Fmi and Gogo do not interact in *trans*. (**j**) Schematic explanation of **f–i**. The red bars indicate the theoretical localization of Fmi if Gogo and Fmi would interact in *trans*, which is not the case. (**k–n**) *gogo*-overexpressing clone (marked by KO) surrounded by *fmi* mutant cells. Fmi localizes on the membrane of Gogo-overexpressing cells between fmi^{+} and fmi^{-} cells (arrowheads), indicating that Fmi and Gogo interact in *cis*. (**o**) Schematic explanation of **k–n**. The red bars indicate relocalized basolateral Fmi in the case of *cis* interaction. (**p–s**) *fmi* mutant R axon clones in third instar larval optic lobe. WT axons are labeled in red, all R axons in blue, Gogo in green. Gogo accumulation is reduced in *fmi* mutant axons (demarcated with dashed white lines). Scale bars represent 10μm.

Figure 6 Gogo and Fmi interact with intracellular components through the Gogo cytoplasmic domain. (**a–c**) Phenotypes of R7 overexpressing Gogo, Fmi and their cytoplasmic truncations. Combinations of overexpressed genes are indicated above each panel by schematics. The labeling is the same as in **Figure 3c–e**. (**a**) Overexpression of GogoΔC and FmiΔIntra. R7s target normally to the M6 layer. (**b**) Overexpression of GogoΔC and Fmi. Few R7s stop at the M3 layer. (**c**) Overexpression of Gogo full length and FmiΔIntra. Almost half of R7s stop at the M3 layer. (**d**) Quantification of the R7 stopping phenotype at the M3 layer. The cytoplasmic domain of Gogo is crucial to generate the R7 premature stopping phenotype.

Figure 7 Fmi is required in target cells for R8 synaptic-layer targeting. (**a**) Medulla of *gcm*-Gal4 $fmi^{-/-}$ FLICK flies. The labeling is the same as in **Figure 1a**. R8s frequently stop at the

M1 layer (arrows). (**b**) Cells that undergo flip-out with *gcm*-Gal4 UAS-FLP are monitored with *Act*<stop<*nLacZ*. Flipped-out cells are labeled with anti-LacZ (green) together with the neuronal marker Elav (magenta). Flip-out occurs in lamina neurons (white arrows), glial cells (arrowheads) and some medulla neurons (yellow arrows), but not in R neurons. (**c**) Quantification of R8 axon bundling and M1 stopping phenotypes in *gcm*-Gal4 $fmi^{-/-}$ FLICK flies. The percentage of stopping axons was assessed by the absence of R8 axons compared to the control flies (asterisk, see also Methods). (**d**–**w**) Fmi expression at 24APF (**d**–**m**) or 48APF (**n**–**w**) in *gcm*-Gal4 $fmi^{-/-}$ FLICK (**d**–**h,n**–**r**) and in the control without FLPase (**i**–**m,s**–**w**). Fmi in *gcm*-Gal4 $fmi^{-/-}$ FLICK medulla (**e,f,o,p**) is significantly reduced compared to the control (**j,k,t,u)**, whereas the level in the lobula stays the same (arrows). The arrowheads indicate the M3 layer. The intensity of the Fmi staining is also indicated in pseudocolors (**g,l,q,v**). The medulla layers (anti-N-Cad) appear normal in *gcm*-Gal4 $fmi^{-/-}$ FLICK flies (**h,r**) compared to the control (**m,w**). (**x**) WT and $fmi^{-/-}$ L3 neurons were marked with GFP using *dac*FLP and an L3 specific Gal4 driver (9-9Gal4). They target their correct layer M3. The scale bars represent 50µm (**b**), 10µm (**d,n**) and 5µm (**x**).

Figure 8 Antagonistic interaction between Gogo and Fmi at the M1 layer. The labeling is the same as in **Figure 1a**. (**a**) Overexpression of Gogo. R8s form blobs at the M1 layer. (**b**) *fmi* hypomorphic FLICK flies. R8 axons bundle to each other with a low frequency and rarely stop at the M1 layer. (**c**) Overexpression of Gogo in *fmi* hypomorphic FLICK flies. R8 axons stop at the M1 layer (arrowheads) more frequently than in *gogo*-overexpressing flies or in *fmi* hypomorphic flies. (**d**) Quantification of the axons stopping at the M1 layer. ($p<0.0001$ Chi-test). (**e**) The moderate overexpression of Fmi using the GMR-*fmi* transgene reduced the number of M1 blobs in Gogo-overexpressing flies (**e**). R8 axons in GMR-*fmi* flies appear normal (**f**). (**g**) Quantification of the blobs at M1 ($p<0.0001$ Chi-test).

METHODS

Methods and any associated references are available in the online version of the paper at http://www.xxxxxxxxxxxxxx

Note: Supplementary information is available on the nature neuroscience website.

Molecular cloning. UAS-Gogo^{Ecto}::Unc5$^{TM+cyto}$-GFP plasmid (residues 1-699 of Gogo and 502-1072 of Unc5) and UAS-SIGHA-Fmi^{EctoΔCad} plasmid (signal peptide from *wg* followed by HA tag and residues 1398-2527 of Fmi) were constructed using standard PCR-based cloning methods and the gateway system (Invitrogen). Unc5 related constructs contain the additional residues SF (HindIII) after the transmembrane domain, since they were amplified from the UAS-SIGHA-Unc5d plasmid[30]. For GMR-*fmi*, NotI-SfiI fragment including full length *fmi* was cut out from CAD47B/pGEM9Zf9(-), subcloned into ENTRY vector, and subsequently recombined into Gateway based CaSpeR-GMR vector. For the BiFC constructs, VN154m9 and VC155 fragments[33] were cloned into the UAST vector. The UAS-Fmi-VN, UAS-Gogo-VC, and UAS-mCD8-VC plasmids were made using standard PCR-based cloning methods.

Fly strains and genetics. Flies were kept in standard *Drosophila* media at 25°C, except for the temporal rescue experiment (27°C and 18°C) and overexpression of *gogo* and *fmi* transgenes (20°C). To perform temporal rescue, flies were shifted from 27°C to 18°C at late 3rd instar larvae. To generate clones overexpressing *gogo* in the wing, flies were heat-shocked for 30min at 37°C at day 3 after egg laying (AEL). To produce *fmi* mutant clones in the wing disc, larvae were heat-shocked for 1hr at 37°C at day 3 AEL. Wing discs were dissected out at 28APF. The following fly stocks and mutant alleles were used: *gogo*[D869], *gogo*[H1675],

gogo[D1600], UAS-*gogo* (T1 and T2), UAS-*gogo*ΔC, *Rh4-mCD8*-4x*GFP*-3x*myc* (abbreviated as Rh4-GFP in the text and the genotype list), *Rh6-mCD8*-4x*GFP*-3x*myc* [18] (abbreviated as Rh6-GFP in the text and the genotype list), *fmi*[E59][21], *fmi*[E86] (hypomorphic allele, D1297N), *eyFLP*2[15], *glass-lacZ*, M(3)i[55][15], FRT80B, FRT42D cl2R11[15], GMR-Gal4, *ey3.5FLP*[31], *ey*3.5Gal80[31], UAS-*mCD8-mKO-myc* (monomeric Kusabira Orange; MBL), GMR-*mCD8-mKO-myc*, GMR-*fmi*, *gcm*-Gal4[26], *Act*<stop<*nlacZ* [32], Df(3L)ED4858, *hsFLP, Act*<*y*$^{+}$<*Gal4*(II), UAS-GFP, Act<CD8<Gal4 (III), Act-Gal4(III), tub-Gal80[ts](II), 109(2)80Gal4, UAS-mCD8GFP, tub-Gal80, UAS-FLP, ap-Gal4[40], dll-Gal4[40], OK107-Gal4[40], c855a-Gal4[41] (Blomington Stock Center), *ppk*-Gal4[27], NP7028[27], *ppk*-EGFP, UAS-*fmi*ΔIntra[29], UAS-*fmi*[21], UAS-*fmi*ΔN::*EYFP*[27], *dac*FLP[38], 9-9Gal4[38], *vang*[stbm-6], *pk*[sple-13][42], *fz*[KD4][43], *dsh*[1], *ato*-τmyc[20], *ato*-Gal4 (gift from K. Senti), UAS-*fz*-EGFP [44]. For the R8 specific rescue of *gogo* mutant, 109-68-Gal4 and *caps*-Gal4[16] were used to achieve R8 specific expression of UAS-*gogo*. For the FLICK technique, two FRT lines (separated by around 100-300kb) flanking a gene to be knocked out were recombined onto the same chromosome. These FRT lines were obtained from Exelixis collection: d10398, f00907, e04690, f03604 and f05961[45]. In heterozygote with the mutation of the gene, FLP was expressed in a desired subset of cells to FLP-out the chromosomal fragment between two FRTs. Thus the gene will be conditionally knocked-out by FLP expression. A more detailed explanation is provided in **Supplementary Figure 2**. For R7 specific co-overexpression, the GMR-FLP technique was used. GMR-FLP induces mitotic recombination only in R1, 6 and R7 [10]. Combining with MARCM (mosaic analysis with a repressible cell marker) system[46], Gal4 expression was induced only in subset of R7s, but not in R8s. The list of detailed genotypes of the flies is provided in **Supplementary Table 2**.

Immunochemistry. Whole mount brain dissection and antibody stainings were done as described [47]. For agarose sections, the proboscis was removed and flies were fixed with 4% formaldehyde overnight. Then, they were embedded in 7.0% standard agarose in PBS at 60-80°C. 50-80 µm sections were cut using a vibrating blade microtome (LeicaVT1000S). This was followed by standard antibody staining procedures. Primary antibodies were used as follows: mAb24B10 (1:50 dilution, DSHB), monoclonal mouse anti-Fmi (#74; 1:20, DSHB), rat anti-Elav (7E8A10; 1:100, DSHB), rabbit anti-Gogo (1:50), rat anti-N-Cad (Ex#8, 1:50, DSHB), rat anti- E-Cad (DCAD2 1:100, DSHB), rabbit anti-GFP conjugated with Alexa488 (1:200, Molecular probe), rabbit anti-Myc (1:200, Gramsch), mouse anti-Myc (9E10, 1:200, Santa Cruz), rat anti-HA (3F10, 1:2000, Roche), rat anti-mCD8 (1;200 Caltag), guinea pig anti-Sens (gift from H. Bellen), rabbit anti-lacZ(1;200, Cappel), mouse anti-LacZ (1:1000, Promega) and chicken anti-lacZ (1:1000, ABcam). Secondary antibodies: Series of Alexa488, Alexa568, Alexa633 conjugated goat anti-mouse, goat anti-rabbit, goat anti-rat, goat anti-chicken secondary antibodies were used (1:200, Invitrogen). EM sections were done according to standard procedures for Drosophila lamina sections. Adult flies were transferred in 70% ethanol for 30s, and heads were cut off in PBS. After removing the proboscis, heads were transferred into the fixative (2.5% glutaraldehyde in PBS) overnight. Heads were then post-fixed in Dalton solution (1% osmium tetroxide, 1% potassium dichromate, 0.85% sodium chloride) and further dehydrated and embedded in Epon. Ultra-thin section (70nm) were obtained with an Ultracut Ultramicrotome (Reichert-Jung) and counterstained with Uranyl acetate and Lead citrate. Images were collected with a magnification of 6000x using Zeiss Em10 and JEOL TEM 1230 microscopes and the number of R cell terminals per cartridge was counted. 66 cartridges were scored in the wild type, 91 in the *gogo* mutant and 57 for the *gogo* R8 specific rescue.

Imaging. Images were obtained with Olympus FV-1000 or Leica SP2 confocal microscopes, and processed with Adobe Photoshop and Illustrator. Notums were imaged with a Leica MZ9$_5$ stereomicroscope attached with a CCD camera (Leica DFC320). Cross section images were created using Imaris software.

Cell culture and transfection

All expression constructs contained the UAS promoter and were co-transfected with pActin5C-Gal4. S2 cells were transiently transfected with Cellfectin (Invitrogen) according to the manufacturer's protocol. Cells were attached to IBIDI slides (μ-slide IV 0.4) for 1hr, fixed for 30min, permeabilized with 0.1% Triton X-100 in PBS, and stained with the following antibodies: with mouse anti-Fmi (#74; 1:50, DSHB), rabbit anti-Gogo (1:20), and rat anti-mCD8 (MCD0800, 1:400, Invitrogen).

Cell aggregation assay.

For the cell-cell contact accumulation assay, 72hr after transfection cells were diluted to obtain a concentration of 10^6 cells/ml and agitated on a rotary shaker for 2hr. To quantify protein accumulation at cell-cell contacts, we used Photoshop to calculate the fluorescence intensities of selected areas at cell-cell borders and on membranes which were not contacting other cells. The background fluorescence was subtracted, and the ratio of the fluorescence intensities between cell-cell contact membranes and free membranes was calculated.

Quantification of midline crossing in md neurons. 20–22hrs AEL embryos were collected on apple juice-agar plates and dechorionated manually. Selected embryos were mounted in glycerol for fluorescence microscopy (Merck). Images were collected with a laser scanning confocal microscopes and processed with Adobe Photoshop (Adobe Systems). Because

dendrites extend on 2D planes just underneath the epidermis, *Z*-series of dorsal front images were projected into 2D images which were then used for quantification.

Lethality test. For the lethality test, we genotyped each mutant animal at first to second instar larval stages using *Kr-GFP*, CyO or *Kr-GFP*, TM3 balancer, and we transfered 20 larvae to a single fresh apple juice plate with a thin spread of yeast paste and raised at 25°C. We counted the number of hatched adults on 14 days AEL for controls and on 17 days AEL for mutants.

Assessment of R8 axonal phenotypes. R8 axons were visualized in confocal-stack images of whole mount brains. (**Fig. 3i**): the number of bundling axons was divided by the total thickness scanned, and the average per 10μm section was calculated. **(Fig. 7c**): although the stopping of R8 axons was clearly visible (see arrows in **Fig. 7a'**), a precise quantification was hampered by the overlapping nature of R8 axons before entering the medulla columns. Therefore, we compared the number of innervating R8 axon between the wild type and the *gcm fmi*$^{-}$ FLICK flies. In the wild type, there are 34.60 R8 axons (Rh6-GFP positive) per 10μm stack (113 μm in total thickness), whereas in *gcm fmi*$^{-}$ FLICK flies, there are 28.38 R8 axons (216μm in total thickness). From these numbers we assessed that 18.0% of R8 axons are stopping at the M1 layer. **(Fig. 8d**): Summation of R8s innervating into the medulla and blobs without axons (arrowheads in **Fig. 8c**) was considered as total R8 axon number. **(Fig. 8g**): percentage of blob-formation per total axon number was calculated. The statistical significance of quantification results was tested using Microsoft Excel.

Co-immunoprecipitation. 48hr after transfection, cells were washed twice in PBS, and lysed with a dounce homogenizer in lysis buffer (1% NP-40, 150mM NaCl, 50mM Tris, pH 7.5) containing protease inhibitors (Roche). After centrifugation at 13,000g for 15min, 250µg of lysate diluted in lysis buffer was incubated with 20µl of anti-myc, anti-V5, or anti-HA agarose beads (Sigma) for 2hr at 4°C. The beads were washed three times with 750µl of lysis buffer and incubated with Leammli loading buffer at 65°C for 30min. The beads were removed by centrifugation and the samples were loaded on a 3-8% Tris-acetate gel (Invitrogen) and analysed by western blotting. Myc-tagged constructs were detected by mouse anti-Myc (9E10, 1:100, Santa Cruz), Gogo-GFP by mouse anti-GFP (JL-8, 1:1000, Clonetech), Fmi-V5 by mouse anti-Fmi (#74; 1:50, DSHB) or mouse anti-V5 (1:5000, Invitrogen), HA-Fmi$^{Ecto\Delta Cad}$ by rat anti-HA (3F10, 1:1000, Roche).

Bimolecular Fluorescent Complementation (BiFC). S2 cells were transfected with VN and VC constructs with *Act*-Gal4 using a low concentration of DNA (0.02µg per well in 24-well plates). 48h after transfection, cells were transferred to slides, fixed, and stained.

Proximity Ligation Assay (PLA)

PLA probes were made for anti-N-Cad (Ex#8, DSHB) and rat anti-mCD8 (MCD0800, Invitrogen) using the Duolink probemaker kit (Olink Bioscience). 72hrs after transfection, cells were fixed as described above and incubated with the PLA probes. The PLA reaction was done according to the DuolinkII Fluorescence protocol (Olink Bioscience).

ACKNOWLEDGEMENTS

We thank Narin Hengrung for helping with BiFC experiments, Igor Siwanowicz for helping with agarose sections and Marianne Braun for EM sections. We thank I. Salecker, T.

Clandinin, J. Axelrod, D. Strutt, B. Dickson, K. Keleman, H. Oda, H. Bellen, J. Morante, J. Smith, DSHB, DGRC Kyoto, Exelixis Collection at Harvard and Blomington Stock Center for reagents, and FlyBase for information resources. We thank Ruediger Klein, Frank Schnorrer, Joachim Egea for suggestions and comments, and the Suzuki lab members for critical discussions. This work was supported by the Max Planck Society and the individual grant from the Deutsche Forschungsgemeinschaft (T.S.).

AUTHOR CONTRIBUTIONS

S. H.-S. conducted the genetic and histological experiments. S. B.-M. conducted the cell culture and biochemical experiments, and assisted the genetic experiments. T. T. conducted the lamina cartridge experiments. T. U., S. H. and T. U. generated and provided the hypomorphic allele of *fmi*. S. H.-S and T. S. designed the experiments. S. B.-M., S. H.-S. and T. S. wrote the paper.

REFERENCES

1. Luo, L. & Flanagan, J.G. Development of continuous and discrete neural maps. *Neuron* 56, 284-300 (2007).
2. Huberman, A.D., Clandinin, T.R. & Baier, H. Molecular and cellular mechanisms of lamina-specific axon targeting. *Cold Spring Harb Perspect Biol* 2, a001743 (2010).
3. Sanes, J.R. & Zipursky, S.L. Design principles of insect and vertebrate visual systems. *Neuron* 66, 15-36 (2010).
4. Sanes, J.R. & Yamagata, M. Many paths to synaptic specificity. *Annu Rev Cell Dev Biol* 25, 161-195 (2009).
5. Yamagata, M. & Sanes, J.R. Dscam and Sidekick proteins direct lamina-specific synaptic connections in vertebrate retina. *Nature* 451, 465-469 (2008).
6. Yamagata, M., Weiner, J.A. & Sanes, J.R. Sidekicks: synaptic adhesion molecules that promote lamina-specific connectivity in the retina. *Cell* 110, 649-660 (2002).
7. Ting, C.Y. & Lee, C.H. Visual circuit development in Drosophila. *Curr Opin Neurobiol* 17, 65-72 (2007).
8. Mast, J.D., Prakash, S., Chen, P.L. & Clandinin, T.R. The mechanisms and molecules that connect photoreceptor axons to their targets in Drosophila. *Semin Cell Dev Biol* 17, 42-49 (2006).

9. Astigarraga, S., Hofmeyer, K. & Treisman, J.E. Missed connections: photoreceptor axon seeks target neuron for synaptogenesis. *Curr Opin Genet Dev* (2010).
10. Lee, C.H., Herman, T., Clandinin, T.R., Lee, R. & Zipursky, S.L. N-cadherin regulates target specificity in the Drosophila visual system. *Neuron* 30, 437-450 (2001).
11. Berger, J., *et al.* Systematic identification of genes that regulate neuronal wiring in the Drosophila visual system. *PLoS Genet* 4, e1000085 (2008).
12. Maurel-Zaffran, C., Suzuki, T., Gahmon, G., Treisman, J.E. & Dickson, B.J. Cell-autonomous and -nonautonomous functions of LAR in R7 photoreceptor axon targeting. *Neuron* 32, 225-235 (2001).
13. Clandinin, T.R., *et al.* Drosophila LAR regulates R1-R6 and R7 target specificity in the visual system. *Neuron* 32, 237-248 (2001).
14. Garrity, P.A., *et al.* Retinal axon target selection in Drosophila is regulated by a receptor protein tyrosine phosphatase. *Neuron* 22, 707-717 (1999).
15. Newsome, T.P., Asling, B. & Dickson, B.J. Analysis of Drosophila photoreceptor axon guidance in eye-specific mosaics. *Development* 127, 851-860 (2000).
16. Shinza-Kameda, M., Takasu, E., Sakurai, K., Hayashi, S. & Nose, A. Regulation of layer-specific targeting by reciprocal expression of a cell adhesion molecule, capricious. *Neuron* 49, 205-213 (2006).
17. Shishido, E., Takeichi, M. & Nose, A. Drosophila synapse formation: regulation by transmembrane protein with Leu-rich repeats, CAPRICIOUS. *Science* 280, 2118-2121 (1998).
18. Tomasi, T., Hakeda-Suzuki, S., Ohler, S., Schleiffer, A. & Suzuki, T. The transmembrane protein Golden goal regulates R8 photoreceptor axon-axon and axon-target interactions. *Neuron* 57, 691-704 (2008).
19. Lee, R.C., *et al.* The protocadherin Flamingo is required for axon target selection in the Drosophila visual system. *Nat Neurosci* 6, 557-563 (2003).
20. Senti, K.A., *et al.* Flamingo regulates R8 axon-axon and axon-target interactions in the Drosophila visual system. *Curr Biol* 13, 828-832 (2003).
21. Usui, T., *et al.* Flamingo, a seven-pass transmembrane cadherin, regulates planar cell polarity under the control of Frizzled. *Cell* 98, 585-595 (1999).
22. Gao, F.B., Kohwi, M., Brenman, J.E., Jan, L.Y. & Jan, Y.N. Control of dendritic field formation in Drosophila: the roles of flamingo and competition between homologous neurons. *Neuron* 28, 91-101 (2000).
23. Chen, P.L. & Clandinin, T.R. The cadherin Flamingo mediates level-dependent interactions that guide photoreceptor target choice in Drosophila. *Neuron* 58, 26-33 (2008).
24. McGuire, S.E., Mao, Z. & Davis, R.L. Spatiotemporal gene expression targeting with the TARGET and gene-switch systems in Drosophila. *Sci STKE* 2004, pl6 (2004).
25. Vladar, E.K., Antic, D. & Axelrod, J.D. Planar cell polarity signaling: the developing cell's compass. *Cold Spring Harb Perspect Biol* 1, a002964 (2009).
26. Ting, C.Y., *et al.* Drosophila N-cadherin functions in the first stage of the two-stage layer-selection process of R7 photoreceptor afferents. *Development* 132, 953-963 (2005).
27. Kimura, H., Usui, T., Tsubouchi, A. & Uemura, T. Potential dual molecular interaction of the Drosophila 7-pass transmembrane cadherin Flamingo in dendritic morphogenesis. *J Cell Sci* 119, 1118-1129 (2006).
28. Chen, W.S., *et al.* Asymmetric homotypic interactions of the atypical cadherin flamingo mediate intercellular polarity signaling. *Cell* 133, 1093-1105 (2008).
29. Strutt, H. & Strutt, D. Differential stability of flamingo protein complexes underlies the establishment of planar polarity. *Curr Biol* 18, 1555-1564 (2008).
30. Keleman, K. & Dickson, B.J. Short- and long-range repulsion by the Drosophila Unc5 netrin receptor. *Neuron* 32, 605-617 (2001).
31. Bazigou, E., *et al.* Anterograde Jelly belly and Alk receptor tyrosine kinase signaling mediates retinal axon targeting in Drosophila. *Cell* 128, 961-975 (2007).
32. Struhl, G. & Basler, K. Organizing activity of wingless protein in Drosophila. *Cell* 72, 527-540 (1993).
33. Saka, Y., Hagemann, A.I. & Smith, J.C. Visualizing protein interactions by bimolecular fluorescence complementation in Xenopus. *Methods* 45, 192-195 (2008).
34. Gajadhar, A. & Guha, A. A proximity ligation assay using transiently transfected, epitope-tagged proteins: application for in situ detection of dimerized receptor tyrosine kinases. *Biotechniques* 48, 145-152 (2010).

35. Shima, Y., *et al.* Opposing roles in neurite growth control by two seven-pass transmembrane cadherins. *Nat Neurosci* 10, 963-969 (2007).
36. Shima, Y., Kengaku, M., Hirano, T., Takeichi, M. & Uemura, T. Regulation of dendritic maintenance and growth by a mammalian 7-pass transmembrane cadherin. *Dev Cell* 7, 205-216 (2004).
37. Grueber, W.B., Jan, L.Y. & Jan, Y.N. Tiling of the Drosophila epidermis by multidendritic sensory neurons. *Development* 129, 2867-2878 (2002).
38. Nern, A., Zhu, Y. & Zipursky, S.L. Local N-cadherin interactions mediate distinct steps in the targeting of lamina neurons. *Neuron* 58, 34-41 (2008).
39. Takemura, S.Y., Lu, Z. & Meinertzhagen, I.A. Synaptic circuits of the Drosophila optic lobe: the input terminals to the medulla. *J Comp Neurol* 509, 493-513 (2008).
40. Morante, J. & Desplan, C. The color-vision circuit in the medulla of Drosophila. *Curr Biol* 18, 553-565 (2008).
41. Fan, Y., *et al.* The egghead gene is required for compartmentalization in Drosophila optic lobe development. *Dev Biol* 287, 61-73 (2005).
42. Tree, D.R., *et al.* Prickle mediates feedback amplification to generate asymmetric planar cell polarity signaling. *Cell* 109, 371-381 (2002).
43. Clandinin, T.R. & Zipursky, S.L. Afferent growth cone interactions control synaptic specificity in the Drosophila visual system. *Neuron* 28, 427-436 (2000).
44. Strutt, D.I. Asymmetric localization of frizzled and the establishment of cell polarity in the Drosophila wing. *Mol Cell* 7, 367-375 (2001).
45. Thibault, S.T., *et al.* A complementary transposon tool kit for Drosophila melanogaster using P and piggyBac. *Nat Genet* 36, 283-287 (2004).
46. Lee, T. & Luo, L. Mosaic analysis with a repressible cell marker for studies of gene function in neuronal morphogenesis. *Neuron* 22, 451-461 (1999).
47. Wu, J.S. & Luo, L. A protocol for dissecting Drosophila melanogaster brains for live imaging or immunostaining. *Nat Protoc* 1, 2110-2115 (2006).

Supplementary Item & Number	Title or Caption
Supplementary Figure 1	Control of the *fmi* transgene expression by the Gal80[ts] system
Supplementary Figure 2	Efficiency of the FLICK system for generating conditional knock-outs.
Supplementary Figure 3	The core PCP complex genes do not regulate R8 axon targeting.
Supplementary Figure 4	R8 projections in *gogo* and *fmi* mutants at different pupal stages
Supplementary Figure 5	Characteristic localization of Gogo in third instar R axons
Supplementary Figure 6	No gain-of-function interaction between *fmi* and *fz*
Supplementary Figure 7	*gogo* and *fmi* mutant phenotypes in R8 axons show a mild qualitative difference at the M1 layer.
Supplementary Figure 8	Gogo does not interact with Fmi in *trans*, nor modulate Fmi-Fmi interaction in *cis*, and Gogo forms oligomers in S2 cells
Supplementary Figure 9	Adherens junctions are not disrupted in *gogo*-overexpressing cells
Supplementary Figure 10	The interaction of Gogo and Fmi do not affect their trafficking nor overall axonal localization

Supplementary Figure 11	Overexpression phenotype and expression of GogoΔC and FmiΔC transgenes.
Supplementary Figure 12	Morphology of the medulla layers in *gcm*-FLICK *fmi*$^{-/-}$ flies.
Supplementary Figure 13	Models for Gogo-Fmi collaboration
Supplementary Figure 14	Co-immunoprecipitation did not show evidence for robust physical interaction.
Supplementary Figure 15	BiFC and PLA showed unspecific interaction on the cell surface
Supplementary Figure 16	The extracellular domain of Fmi is required for R8 axon targeting.
Supplementary Figure 17	Fmi can be detected on R axons in the mid-pupal stage.
Supplementary Table 1	Gal4 strains used for FLICK in the target area of R axons
Supplementary Table 2	The genotypes of the flies
Supplementary Note 1	Consideration on methods for detecting the physical interactions of Gogo and Fmi

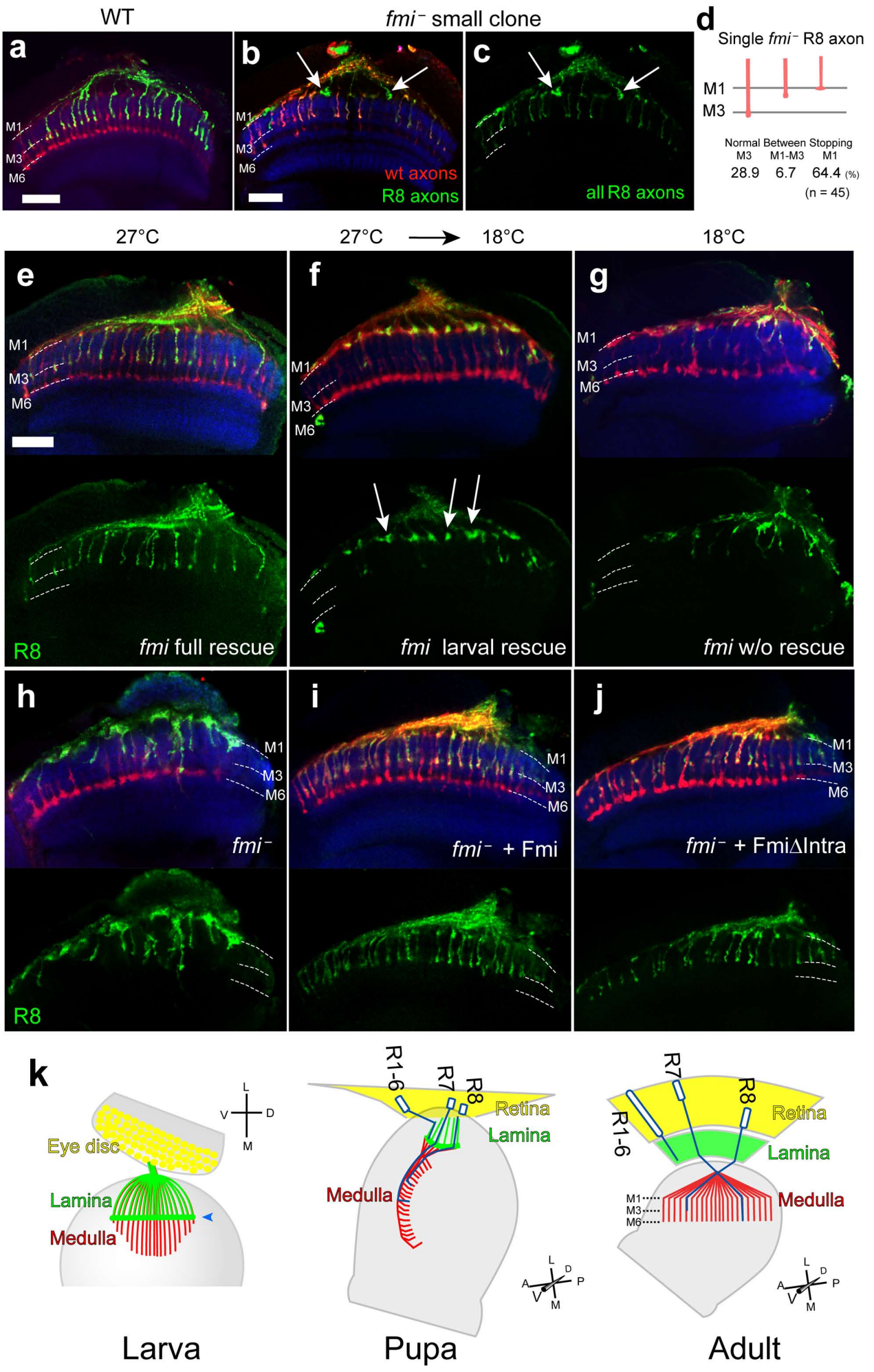

Figure-1(Suzuki)

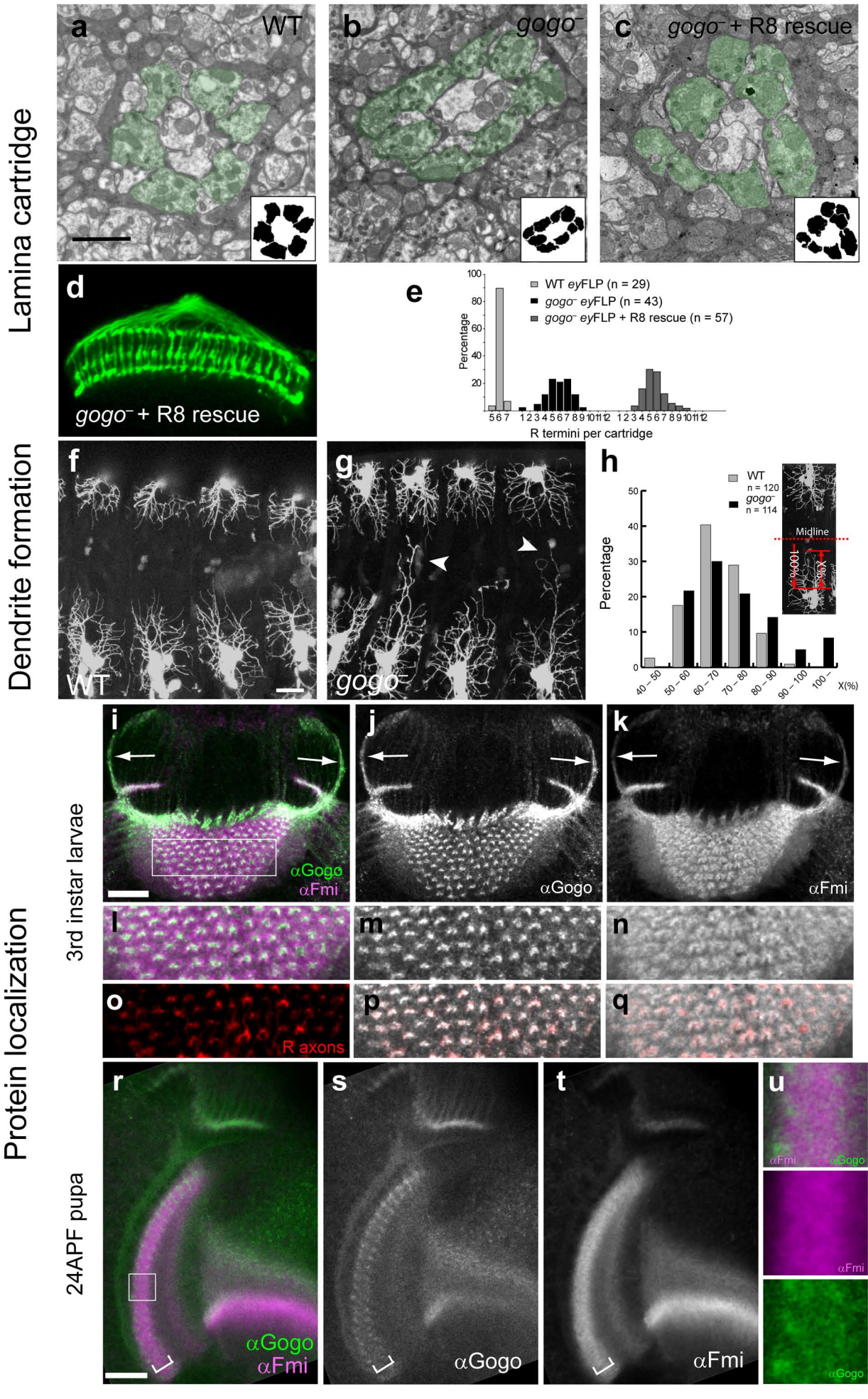

Figure-2 (Suzuki)

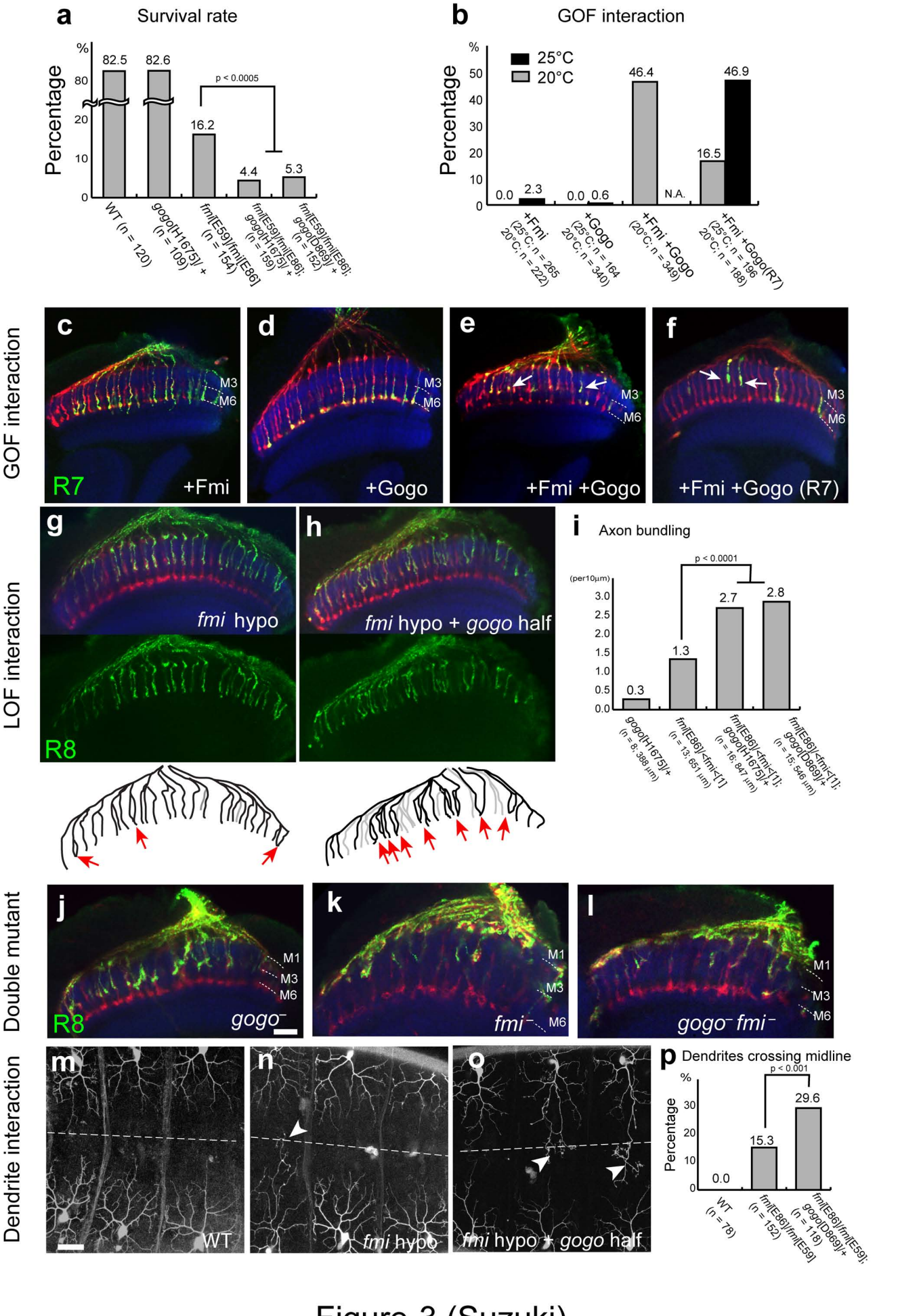

Figure-3 (Suzuki)

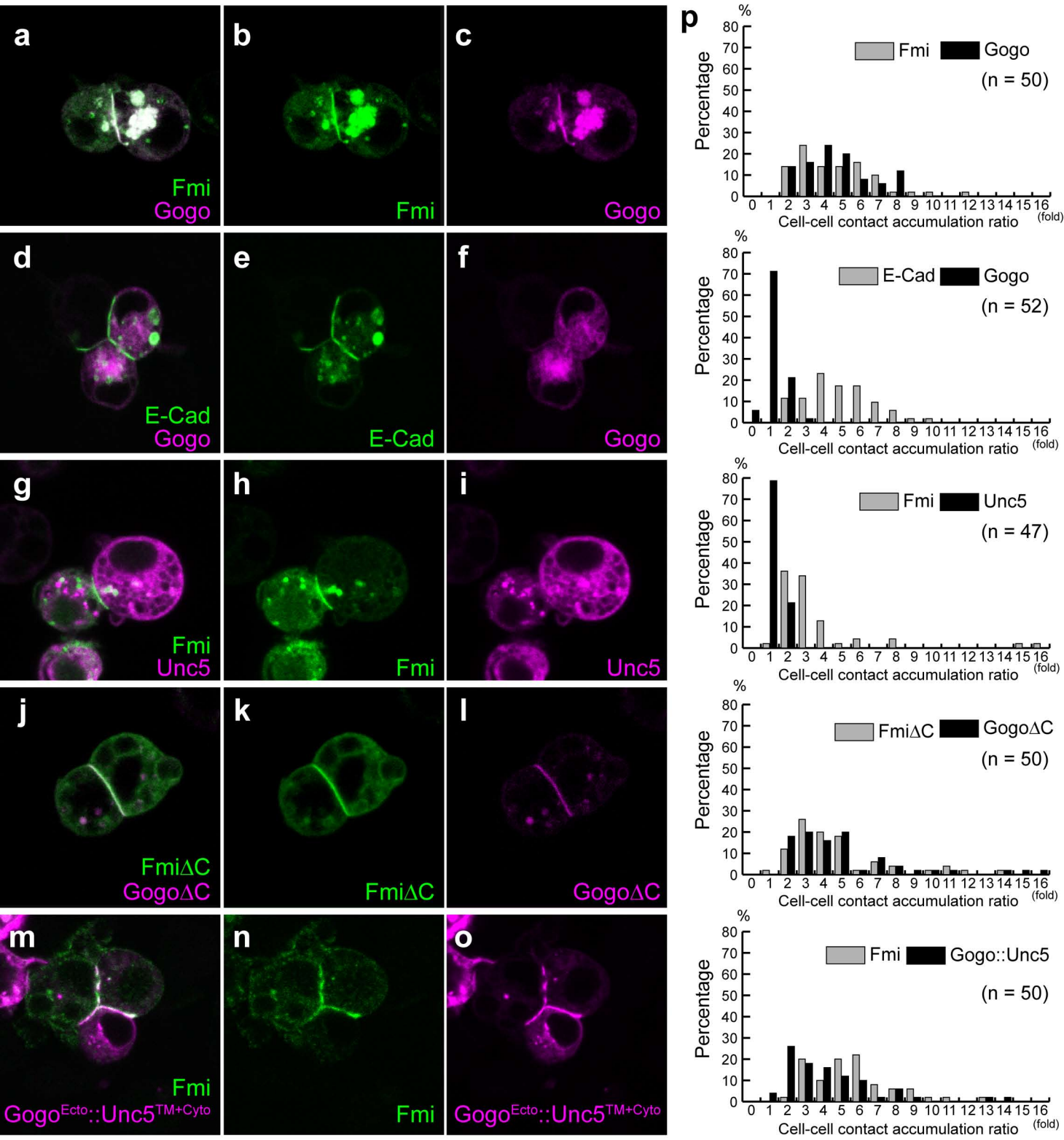

Figure-4 (Suzuki)

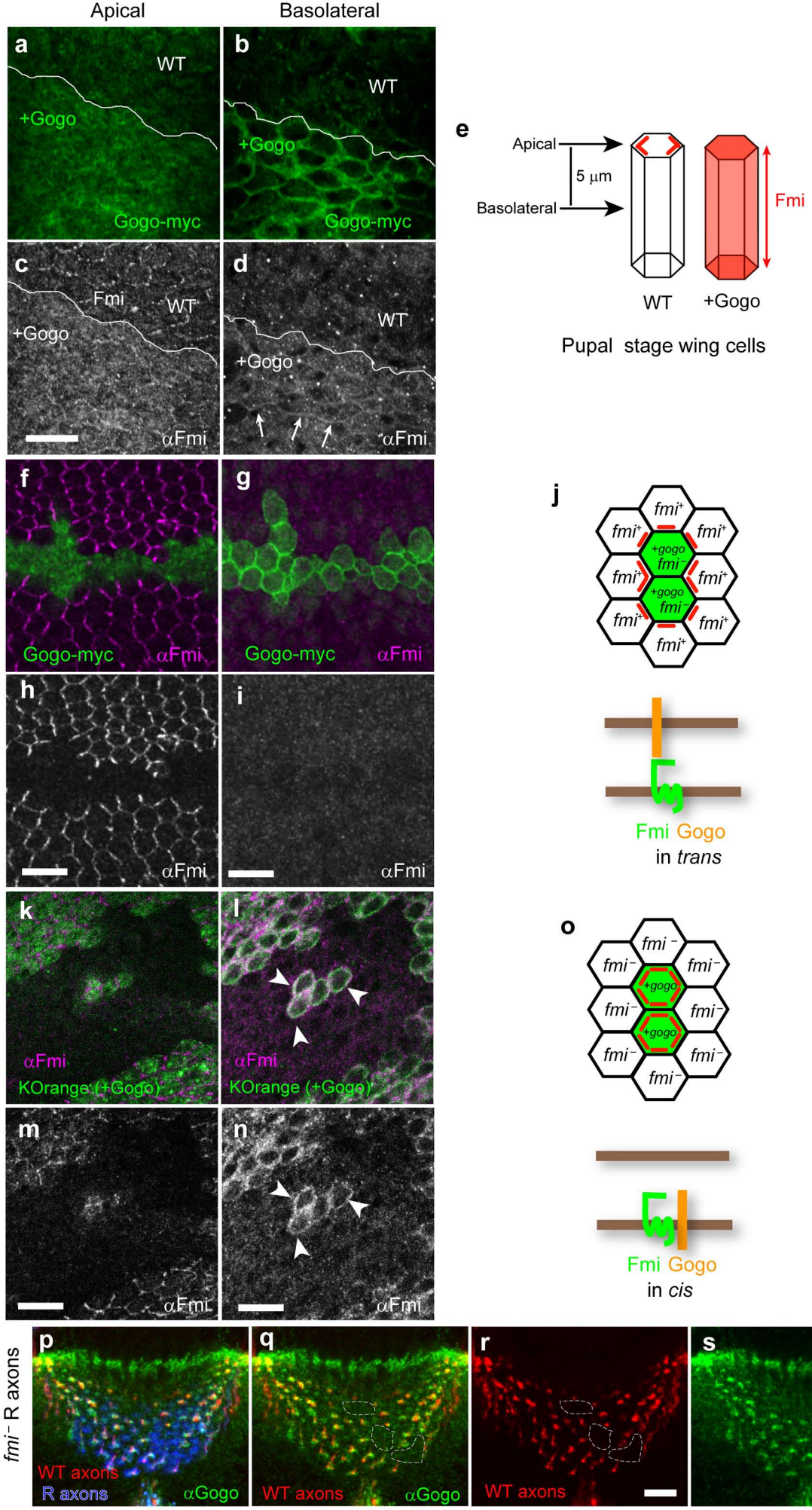

Figure-5 (Suzuki)

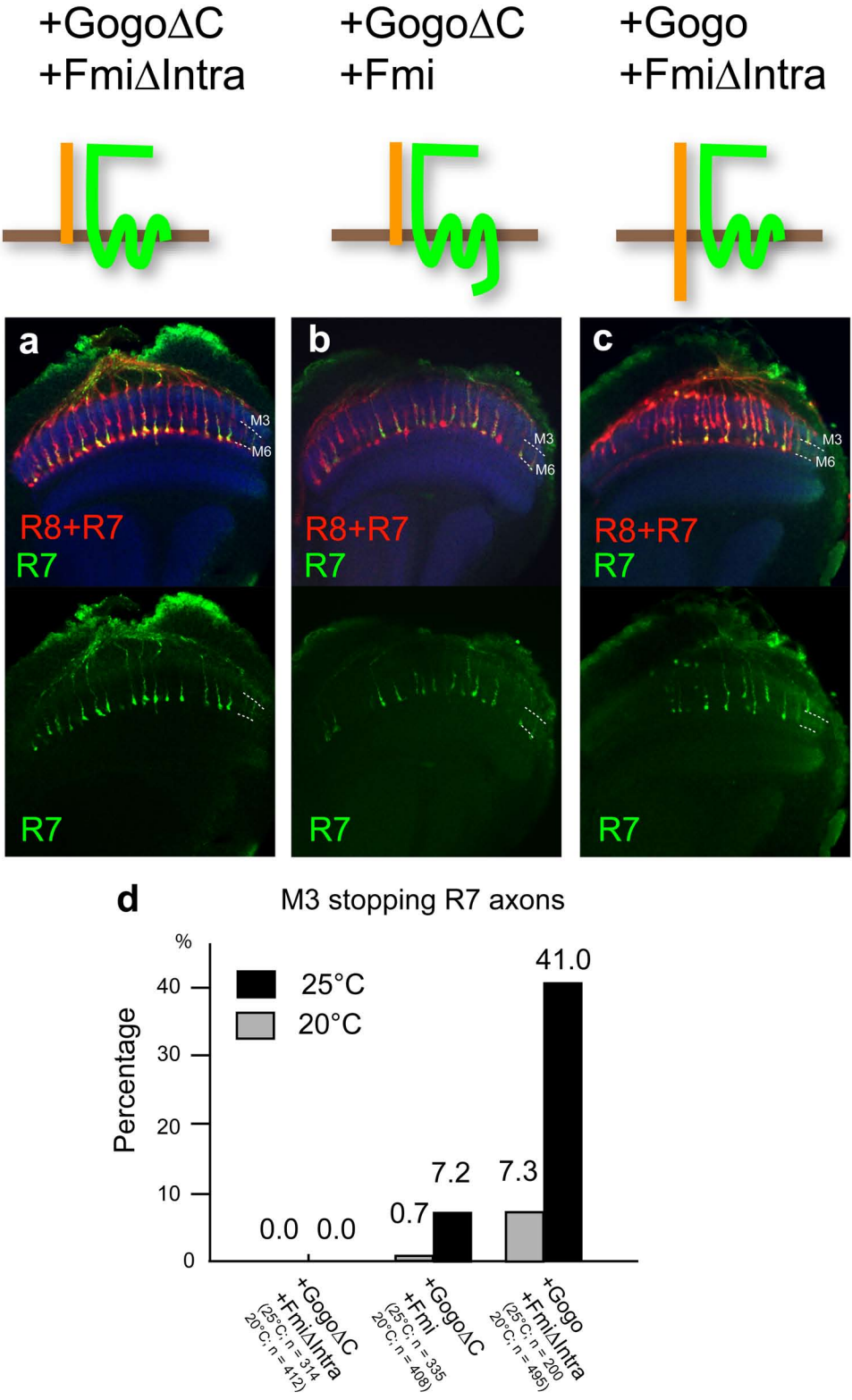

Figure-6 (Suzuki)

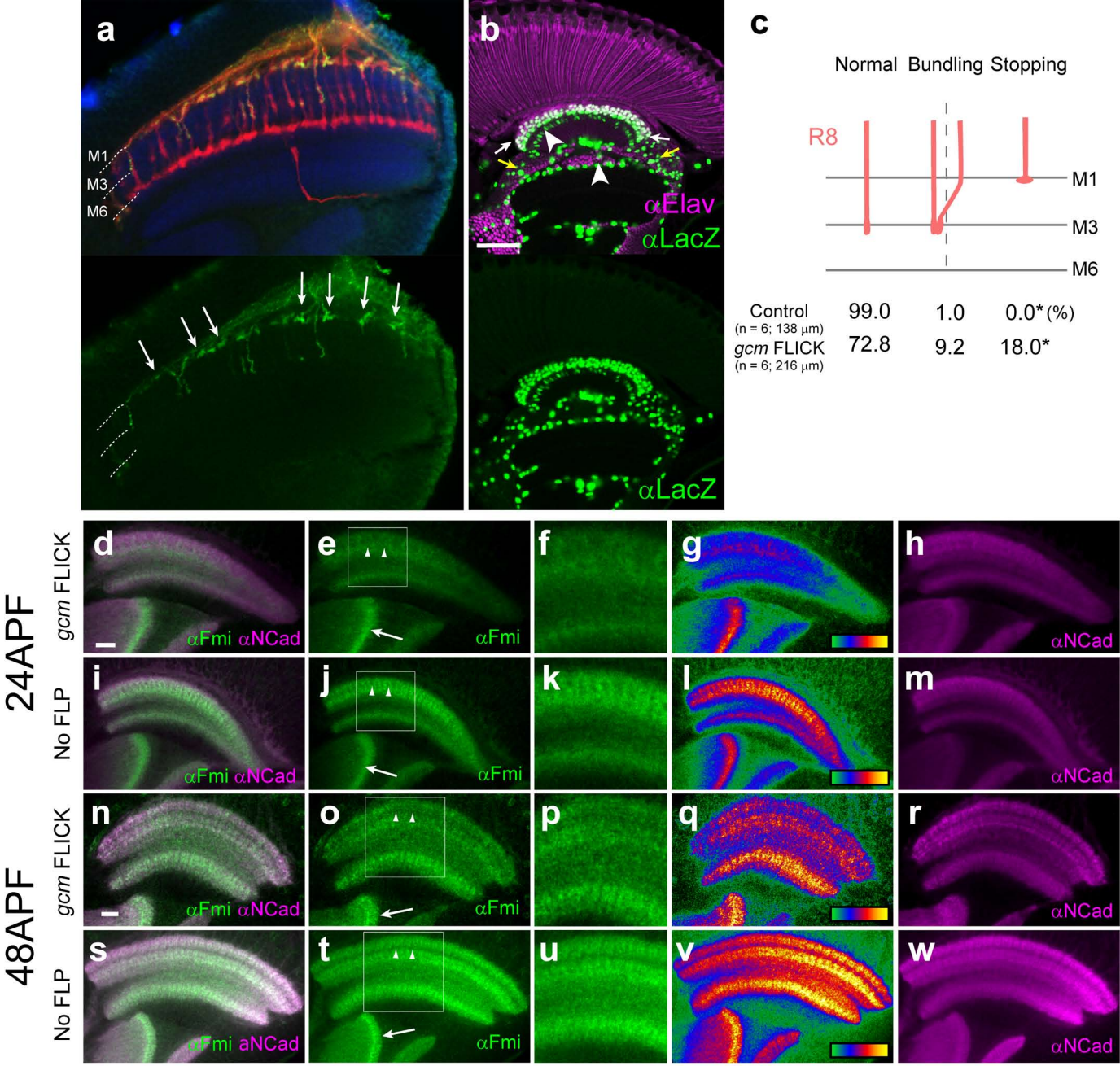

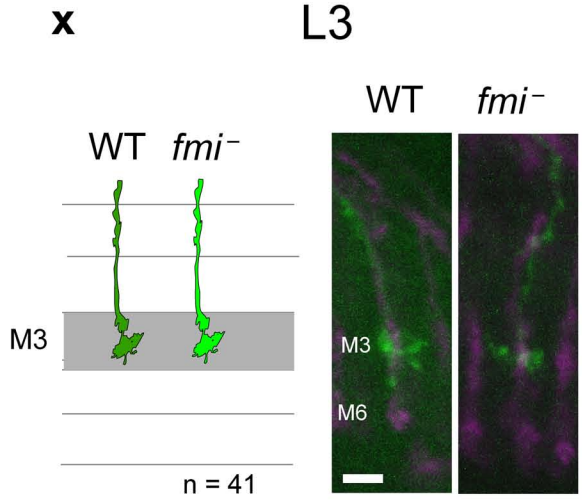

Figure-7 (Suzuki)

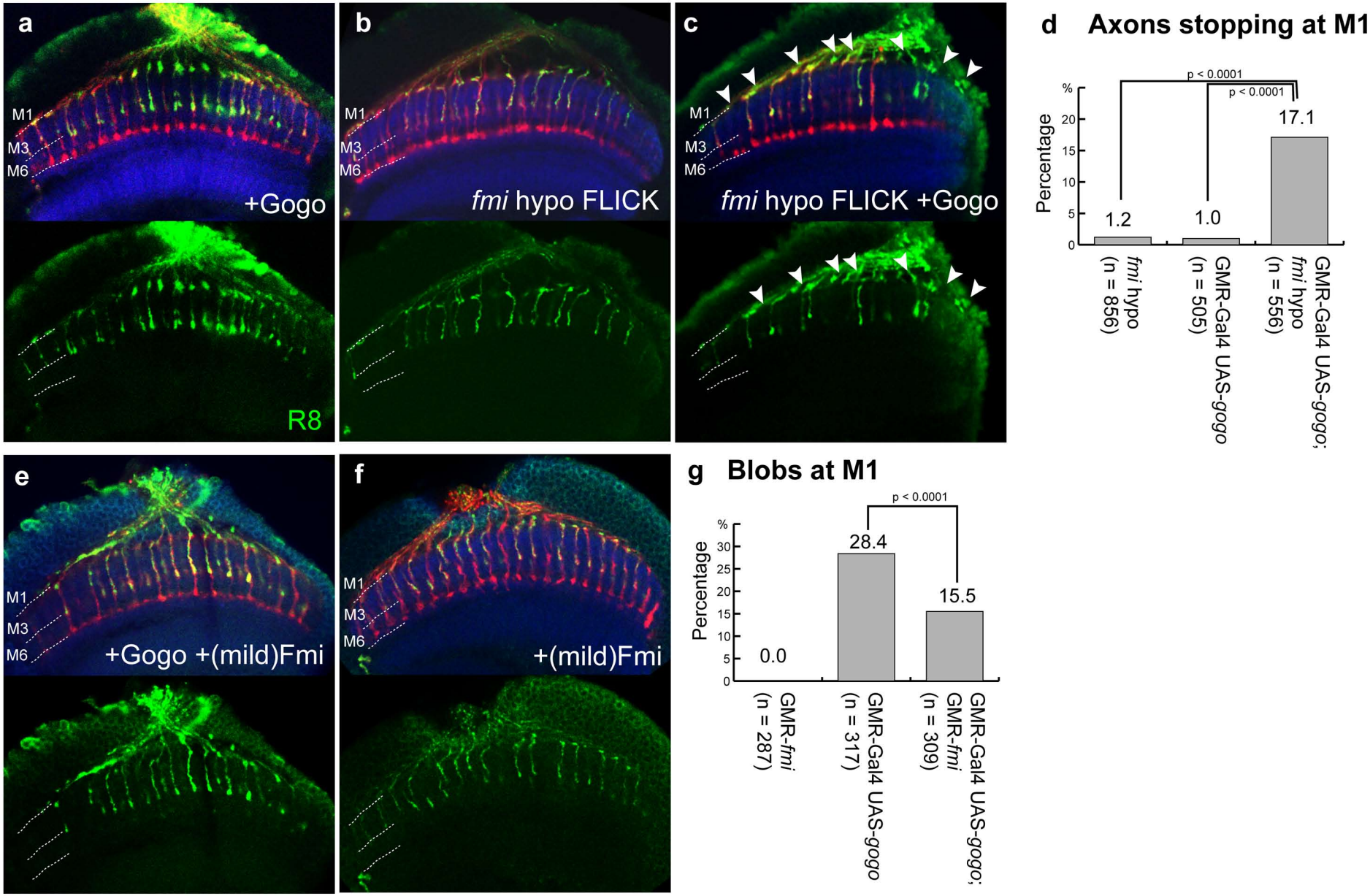

Figure-8 (Suzuki)